Electrostatic ion beam trap for electron collision studies

O. Heber
Department of Particle Physics, Weizmann Institute of Science, Rehovot, 76100, Israel

P. D. Witte
Department of Particle Physics, Weizmann Institute of Science, Rehovot, 76100, Israel and Max-Planck-Institut für Kernphysik, D-69117 Heidelberg, Germany

A. Diner, K. G. Bhushan,[a] D. Strasser, and Y. Toker
Department of Particle Physics, Weizmann Institute of Science, Rehovot, 76100, Israel

M. L. Rappaport
Physics Services Unit, Weizmann Institute of Science, Rehovot, 76100, Israel

I. Ben-Itzhak[b]
Department of Particle Physics, Weizmann Institute of Science, Rehovot, 76100, Israel and J.R. MacDonald Laboratory, Physics Department, Kansas State University, Manhattan, Kansas 66506

N. Altstein
Department of Particle Physics, Weizmann Institute of Science, Rehovot, 76100, Israel

D. Schwalm and A. Wolf
Max-Planck-Institut für Kernphysik, D-69117 Heidelberg, Germany

D. Zajfman
Department of Particle Physics, Weizmann Institute of Science, Rehovot, 76100, Israel and Max-Plank-Institut für Kernphysik, D-69117 Heidelberg, Germany

(Received 29 July 2004; accepted 3 October 2004; published online 20 December 2004)

We describe a system combining an ion beam trap and a low energy electron target in which the interaction between electrons and vibrationally cold molecular ions and clusters can be studied. The entire system uses only electrostatic fields for both trapping and focusing, thus being able to store particles without a mass limit. Preliminary results for the electron impact neutralization of C_2^- ions and aluminum clusters are presented. © *2005 American Institute of Physics.*
[DOI: 10.1063/1.1832192]

I. INTRODUCTION

The interaction of electrons with molecular ions is a fundamental process which takes place in many natural environments. Probing such interactions contributes not only to better understanding of various plasma environments on the basis of elementary reactions, but also to the understanding of basic physical concepts behind the dynamics of molecular processes. The main experimental limitation in the study of elementary collision processes with molecular ions typically arises from the lack of control over the initial internal temperature (electronic, vibrational, and rotational excitation) of the species under study. Standard ion sources tend to produce molecular ions with relatively high internal temperature, while the comparison of experimental data with theoretical predictions, as well as their significance for cold environments such as astrophysical plasmas requires that measurements be made under controlled conditions, i.e., with well-defined initial states or with molecular samples of low internal temperature.

Energy-resolved studies in this field were performed using crossed electron and molecular-ion beams, ranging from the earliest works in the late 1970s[1,2] and up to very recent studies.[3–5] However, internal excitation of the molecular ions introduces substantial ambiguities in the interpretation of these experiments, especially at collision energies of the order of 10 eV or below. During the last decade, studies of electron impact processes on internally cold molecular ions could be realized by using magnetic heavy-ion storage rings.[6–8] Here, molecular ion beams of MeV energies are stored over times long enough to allow for radiative decay of the internal excitation produced in the ion source, yielding cold (300 K) molecular ions; in addition, by using the merged beams technique the interaction of these ions with free electrons can be measured down to zero collision energy with an energy resolution approaching 1 meV (Ref. 9) in some cases. This technique also offers very favorable conditions for absolute cross section measurements, as the merged beam geometry and the kinematical cooling of the ion beam by collisions with the equivelocity electrons in the storage ring ensure a well-controlled beam overlap (form factor). On the other hand, many advantages of the merged beams technique as applied at the existing magnetic storage rings depend on the relatively high ion beam velocity which allows

[a]Present address: Technical Physics Division, Bhabha Atomic Research Center, Trombay, Mumbai 400085, India.
[b]Varon Visting Professor.

one to produce equivelocity electron beams at convenient laboratory energies ($\gtrsim 10^2$ eV). Given the available magnetic bending powers, the maximum ion beam velocity rapidly decreases for molecular ions and clusters of increasing mass. Thus, although experiments with clusters as heavy as C_{86}^- have been performed in storage rings,[10] no electron impact experiments have been performed on clusters heavier than C_4^-.[11] More importantly, systematic studies as a function of the cluster size (i.e., the number of atoms in a cluster), are difficult to perform with magnetic rings due to the complexity of the ring tuning for each independent mass.

To overcome these limitations, electrostatic ion storage devices have started to appear during the last few years; they include the electrostatic storage rings at the University of Aarhus [ELISA (Ref. 12)] and at KEK (Ref. 13) and the electrostatic ion beam trap.[14,15] Being electrostatic, these devices can store ion beams of a given kinetic energy independently of the ion mass, allowing operation over a virtually unlimited mass range. They already have provided new opportunities for experiments with cold, very heavy molecular ions,[16,17] including the use of an electron target[18] at ELISA and even an electron cooler[17] at the KEK electrostatic ring.

In this paper, we present a new crossed-beam setup comprising an electrostatically focused electron beam target installed inside an electrostatic ion beam trap.[14,15,19,20] In this compact arrangement (overall size $\sim$1 m) keV ions can be stored for times that are sufficient to achieve internal relaxation, and neutral products resulting from the interaction with electrons at controlled energies of $\sim$5 to 100 eV can be observed. The purely electrostatic operation which, in contrast to the recent arrangements at Aarhus and KEK,[17,18] avoids any magnetic fields in confining the low-energy electrons, makes it possible to realize the interaction with the crossed electron beam essentially independently of the ion mass for a wide spectrum of heavy molecular ions and charged clusters. Strict mass independence holds in particular for the ion optics in the trap, even in the presence of the electron beam; neither the ion trap nor the electron beam have to be retuned when changing from one ion species to another, using the same acceleration energy at the ion source. This ensures a constant beam-overlap factor, which makes the system particularly well-suited for the systematic study of electron collision cross sections as functions of the ionic size or composition. A description of the electrostatic ion beam trap is given in Sec. II, while the characteristics of the electron target are given in Sec. III. Procedures for the measurement of electron collision cross sections are described in Sec. IV, and preliminary results on electron impact detachment of stored negative aluminum clusters and C_2^- are given in Sec. V.

II. THE ELECTROSTATIC ION BEAM TRAP

The trap used in this work is an enhanced version of the electrostatic trap described in Refs. 14 and 15. The trap has two electrostatic mirrors facing each other, each made of 8 electrodes, identical to those described in Refs. 14 and 15; the distance between the innermost electrodes is 490 mm (see Fig. 1). The mirrors are installed on a custom-made

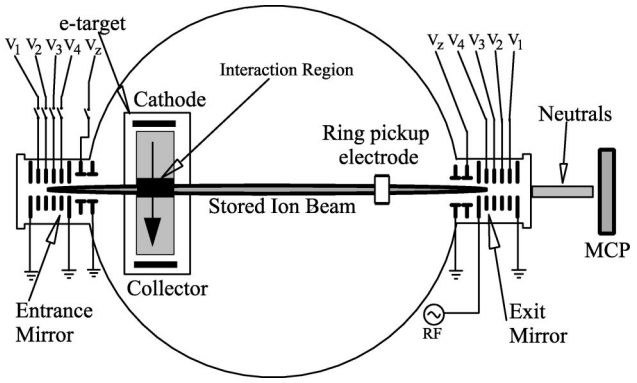

FIG. 1. Schematic drawing of the electrostatic trap and electron target.

optical table inside a squat, cylindrical chamber with inner diameter of 451 mm. The mirrors, as well as all other components screwed to the table, are positioned without any adjustment to an accuracy of ± 50 μm thanks to the precisely spaced array of reamed holes. The table stands on three blocks bolted to the floor of the chamber in the manner of a kinematic mount (see Fig. 2). The chamber is pumped from below by a 2000 l/s cryopump (see Fig. 3), and by three additional nonevaporable getter (NEG) pumps.[21] Two of the NEG (SAES - SORB-AC WP750) pumps are screwed to the table between the electron-beam target and the entrance mirror (see Sec. III C), while the third flange-mounted pump (modified version of SAES - Capacitorr 2000-D MK5) is on a port normal to the trap axis near the trap center. Two additional cryopumps are located on the beam line leading to and exiting from the scattering chamber, and a third is mounted to one of the chamber's ports. After activating the getter pumps and baking, a background pressure lower than 7×10^{-12} Torr is measured using an ion gauge located on top of the chamber.

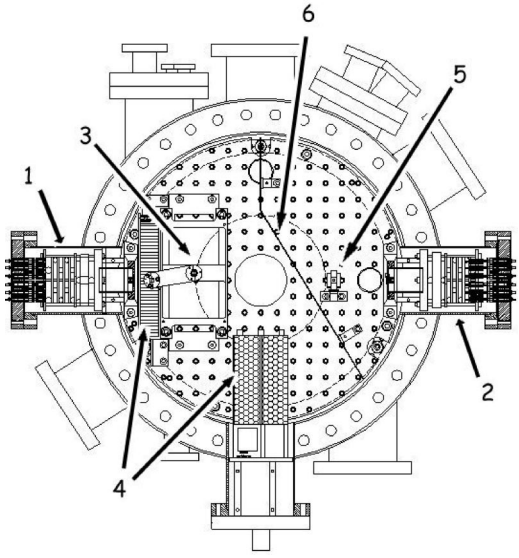

FIG. 2. Layout (top view) of the scattering chamber. (1) Entrance mirror, (2) exit mirror, (3) electron target, (4) getter pumps: NEG SORB-AC WP750 (Left) and NEG Capacitor 2000-D MK5 (right), (5) pickup electrode, (6) electron shield. The mirrors, flange-mounted NEG pump and their ports, are shown in horizontal section through the trap axis. (See Fig. 3 for a vertical section through the trap axis.)

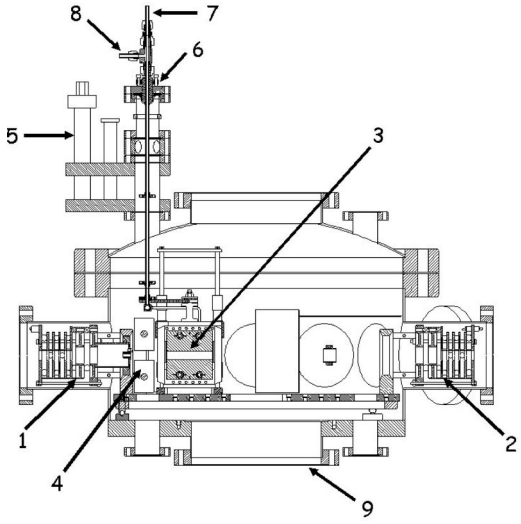

FIG. 3. Vertical section (through mirror axes) of the scattering chamber: (1) Entrance mirror, (2) exit mirror, (3) electron target mounted on its frame, (4) getter pumps, (5) manipulator used to raise the electron target, (6) electrical feedthroughs for electron target electrodes, (7) input tube for water-cooling of cathode support (-50 V), (8) outlet for water-cooling, and (9) port for cryopump.

Various voltages can be applied to the electrodes of the trap in order to achieve stable confinement, for which the stability conditions have now been well studied.[19,20] For the data presented in Sec. IV and V, the 4.2 keV anions were trapped with the following potentials (see Fig. 1): $[V_1, V_2, V_3, V_4, V_z] = [-6.48\ \text{kV},\ -4.67\ \text{kV},\ -3.83\ \text{kV},\ -2.75\ \text{kV},\ -1.75\ \text{kV}]$. Because the two innermost electrodes are grounded, the central region of the trap is field-free. Ions are injected into the trap by lowering the voltages on the entrance electrodes (on the left hand side of Figs. 1 and 2). More details about the operation of the trap and its characteristics can be found in Refs. 19 and 20.

A pickup ring, located between the two mirrors (see Figs. 1 and 2), is used to measure the number of ions in the trap in a bunched mode.[20] The signal induced on the pickup by the passage of a bunch of ions is amplified by a charge sensitive amplifier and fed to a digital scope. Fourier analysis of the signal gives both the frequency of oscillation and the amplitude, which is proportional to the number of stored ions. In the present case, bunching is achieved by applying a small rf voltage to one of the electrodes of the exit mirror, with a frequency that is equal to the natural oscillation frequency of the particles in the trap ($\sim$100 kHz) and an amplitude of 10 V peak-to-peak. The amplitude of the rf signal is raised slowly ($\sim$120 ms) after the injection in order to reduce ion losses. More details about the use of the pickup are given in Sec. IV C. Neutral clusters or fragments produced in the trap while the ions are moving toward the exit side, either via collisions with the residual gas (background), or because of interactions with the electron beam (signal), are detected by a 40 mm diam. microchannel plate (MCP) detector located 0.85 m downstream from the exit of the trap.

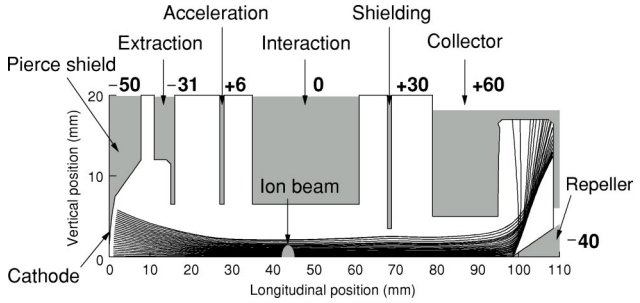

FIG. 4. Section along the vertical midplane of the electron target (upper half, with mirror symmetry about the horizontal plane) together with a two-dimensional space-charge flow simulation of electron trajectories with zero initial velocity at the cathode, using the SLAC Electron Optics Program (Ref. 24) (mesh size 0.5 mm). The electrode voltages (bold numbers) are given in volts for an acceleration voltage of $U_0 = 50$ V. The calculated perveance per unit length of the cathode (assuming infinite extension perpendicular to the simulation plane) is 0.268 μA $V^{-3/2}$ cm^{-1}.

III. ELECTRON GUN TARGET

A. Constraints and requirements

The electron target is located in the field-free region between the two electrostatic mirrors, closer to the entrance electrodes. It produces an electron beam of rectangular cross section crossing the trap axis (see Fig. 1). Neutral products from the electron-ion interaction region leave the trap on straight trajectories and are detected by a multichannel plate (MCP) detector behind the trap. Operation at energies from $\sim$50 eV down to about 5 eV is possible; these energies correspond approximately to the collision energy in the center-of-mass frame because the velocity of the trapped ions is much smaller than that of the electrons.

Two important requirements had to be taken into account while designing the electron target. The first was that no external electric or magnetic fields should be present in the interaction region where the electron and ion beams cross, so as to avoid perturbation of the ion motion in the trap. Thus, the magnetic field that is commonly added to guide the electrons could not be used in the present configuration. The second requirement was to obtain the highest possible electron densities while the background pressure in the trap remains low ($\lesssim 5 \times 10^{-11}$ mbar) in order to ensure a sufficient lifetime of the ion beam in the trap and a small background rate at the MCP detector of neutral particles produced by ion collisions with the residual gas.

B. Design

The electrode configuration of the electron target[22] is shown in a vertical section perpendicular to the stored ion beam in Fig. 4. The electrons are produced by a rectangular cathode (12×50 mm) with a concave emission surface of 20 mm radius of curvature. The ion beam crossing position is in a field free region 43 mm from cathode, between grounded electrodes spaced 13 mm apart and 28 mm long. To guarantee overlap the trapped ion beam whose diameter is $\sim$3 mm, the vertical extent of the electron beam must be at least 5 mm. For the nominal operating conditions, the emission current I is given in terms of the voltage U_0 between the cathode and the interaction region as

$$I = P_0 U_0^{3/2}, \tag{1}$$

where $P_0 = 1.34\ \mu\text{A V}^{-3/2}$ is the value of the beam perveance calculated by the space-charge flow simulation shown in Fig. 4 for a cathode length of 50 mm perpendicular to the simulation plane. The chosen perveance P_0 is about a factor of 5 below the maximum space-charge limited perveance[23] for electron transport through the gap between the interaction electrodes. In combination with adequate focusing in the acceleration region, this makes it possible to maintain an almost uniform space-charge flow through the interaction zone.

The field shaping electrodes were first optimized using simulations of the electron trajectories by the SLAC Electron Optics Program for 2D calculation,[24] including the external electric fields as well as the electron space-charge field (Fig. 4). The electrons are accelerated from the cathode in space-charge limited emission perpendicular to the active surface. The effective accelerating field, including the space-charge effect, is appropriately shaped by Pierce shields kept at the same potential as the cathode and meeting its upper and lower edges at an angle of 22.0° (optimized angle according to the simulations, lying close to the value of 22.5° for a planar cathode-anode geometry[25]). The emission current is mainly determined by the extraction electrode, located ~15 mm from the cathode and having a potential of 38% of the total acceleration voltage for the nominal perveance P_0. Further acceleration towards the interaction region takes place up to a distance of ~30 mm from the cathode. For lower electron extraction voltage, hence lower space charge fields, the acceleration geometry yields a focus at ~30 mm from the cathode. For extraction voltages higher than nominal the increased space charge leads to a diverging beam in the interaction region. The standard field geometry, used throughout the measurements described here, is produced by the voltages as given in Fig. 4 for an electron energy of $E = eU_0 = 50$ eV. For different electron energies all voltages are scaled linearly. This leads to an identical space-charge flow at all energies, with the beam current scaling according to Eq. (1).

Following the 2D simulations, the end effects resulting from the finite length of the electrodes (i.e., normal to the plane of Fig. 4) were studied[22] in 3D calculations, using space charge trajectory simulations with the MAFIA4 code.[26] The defocusing effects in the end regions shown by these simulations (Fig. 5) were minimized by using additional shielding electrodes at the cathode potential near the cathode edges; re-focusing effects near the interaction region could be obtained by choosing the acceleration electrode on both sides ~5mm narrower (in ion beam direction) than the other electrodes. The 3D calculations predict an overlap length with the ion beam of close to 60 mm for a cathode length of 50 mm. The predicted perveance of the 3D calculations of $1.32\ \mu\text{A V}^{-3/2}$ is practically identical to the 2D result given above.

The electrons are produced from a dispenser-type cathode[27] of type 532 (derived from the impregnant composition of 5 BaO:3 CaO:2 Al_2O_3) with an osmium–ruthenium (M-type) coating which allows the cathode to be operated at lower temperatures than standard dispenser cathodes. The relatively small emission current output required for the present application ($<1\ \text{mA/cm}^2$) could be obtained at an operating temperature of 800 °C which helped in reducing the load on the vacuum system. The cathode assembly[28] has a noninductive (bifilar) heater and only nonmagnetic materials are used to ensure minimal distortion of the electron beam.

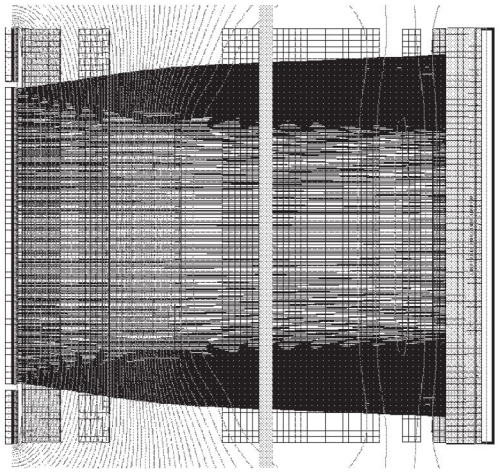

FIG. 5. Horizontal section through simulated electron trajectories (black) and potential lines (gray) in the midplane of the electron target, as obtained from a three-dimensional space-charge flow calculation using the MAFIA4 code (voltage step of the equipontentials: $U_0/50$ V; cathode width: 50 mm). The cathode (left) and the electrodes are shown by cross-hatched area. The gray vertical line indicates the approximate ion beam position.

At the low beam energies used here and through the absence of a magnetic guiding field, relatively large beam spreading due to the initial thermal velocities of the electrons is expected. The root-mean-square (rms) electron velocity spread $\sigma_v = (kT/m)^{1/2}$ in a single degree of freedom amounts to $1.28 \times 10^7 \text{cm/s}$ at the operating temperature of 800 °C ($kT = 0.092$ eV). Taking into account the variation of the accelerating field along the beam direction, the electron travel times from the cathode to the ion beam position (43 mm), to the end of the interaction electrode (63 mm) and to the shielding electrode in front of the collector (68 mm) are 22 ns, 27 ns, and 28 ns, respectively, at an acceleration energy of $E = 50$ eV. Modeling the thermal effects by free propagation perpendicular to the simulated beam trajectories, rms spatial spreading amounting to 2.8 mm, 3.5 mm, and 3.6 mm, respectively, is obtained at the given positions. This spreading, which scales as $\propto (50\ \text{eV}/E)^{1/2}$, is substantial in comparison to the beam width of 4–5 mm obtained from the "laminar"[23] space-charge flow simulations that neglect thermal effects. Test measurements of the electron beam profile described below are consistent with this simple estimate.

After leaving the interaction region the electrons enter a collector kept at positive voltage with respect to the interaction region. A positive collector potential and the special shape of the collector and repeller were chosen to minimize possible leakage of secondary and backscattered electrons into the interaction region. The shielding electrodes ensure that the accelerating field of the collector does not penetrate

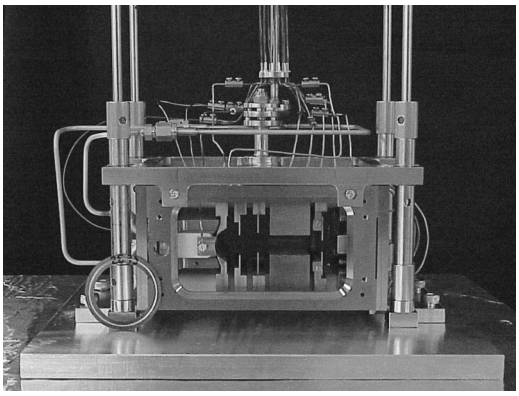

FIG. 6. Photograph of the electron target with its vertical guide rods. The cathode is on the left and the collector is on the right. The stored ion beam passes between the two massive electrodes, perpendicular to the figure plane. The O.D. of the gasket leaning against the lower left corner of the target is 48 mm.

into the interaction region. The shielding electrodes define an entry slit into the collector with a height of 7.5 mm.

C. Construction

The electrodes and the frame of the electron target[22] were made of titanium. Titanium was chosen because of its low outgassing when heated by radiation from the cathode, and because its thermal expansion coefficient is almost identical to the diamond-turned ceramic rods used for suspension of the electrodes. For the less critical collector, stainless steel was used for ease of manufacturing. The cathode is mounted on a water-cooled copper block. The water tubes serve as one of the high current leads to the cathode and are therefore at the cathode potential. A photograph of the electron target assembly is shown in Fig. 6.

The electron target assembly is mounted so that vertical scanning of the electron beam is possible using an external manipulator. This was used for verifying the overlap between the ion and electron beams. The electron target is suspended from a support structure that moves on four stainless steel shafts using linear ball bearings. Figure 3 shows the side view of the electron target installation including the feedthrough arrangement.

The ion trap setup is surrounded by a set of coils used to compensate the earth magnetic field. They are adjusted for optimal electron collection efficiency at low acceleration voltages. Small stray electric fields, in particular those originating from the positive fields used to trap the ion beam, can easily deflect electrons from the edges of the ribbon electron beam and hence had to be carefully screened. Electrons accelerated towards the positive trap electrodes, kept at keV voltages, were in particular found to produce background on the MCP detector used for the neutral products. To avoid this, a shield was added (see Fig. 2), separating the electron target from the exit side of the trap. A 10 mm hole in the shield allowed passage of the stored ion beam.

D. Electron gun operation

After assembly the electron target was tested in standalone operation at pressures of $\sim 10^{-8}$–10^{-7} mbar. The emission current and the currents arriving at all electrodes were measured as functions of the acceleration voltage U_0 in the range of 5–50 V. Moreover, the sensitivity of the beam propagation, as revealed by the electrode currents, to external magnetic fields was investigated, and the beam profile was imaged at an energy of 50 eV using a phosphor screen.

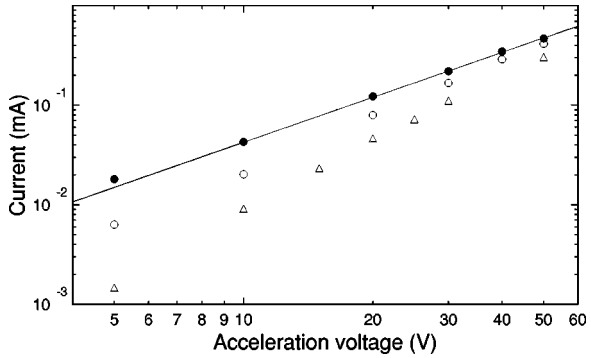

FIG. 7. Emission current from the cathode (filled circles), current transmitted through the interaction electrodes (open circles) and collector current (open triangles) measured as a function of the acceleration voltage U_0. The line shows the prediction of Eq. (1) with $P_0 = 1.34\ \mu\mathrm{A\ V}^{-3/2}$.

Varying all applied voltages proportionally to U_0, the emission current was found to follow well the scaling law of Eq. (1) for space-charge flow with the beam perveance P_0 very close to the predicted values of Sec. III B, as shown in Fig. 7. Part of the electron current through the interaction region arrives at the shielding electrodes in front of the collector, while the majority arrives at the collector itself. The sum of these currents as well as the collector current alone (i.e., the current passing through the gap of 7.5 mm between the shielding electrodes) are also shown in Fig. 7. At 50 eV, $\sim$90% of the emission current is transmitted through the interaction electrodes, though only $\sim$60% of the current is found at the collector, in contrast to the space-charge flow simulation. For lower U_0, both the relative collector current and the transmitted current ratio decrease further (see Fig. 8). The measured current ratios compare reasonably well with the predicted trend of the thermal effects discussed in Sec. III B. To model these effects, a (normalized) rectangular cur-

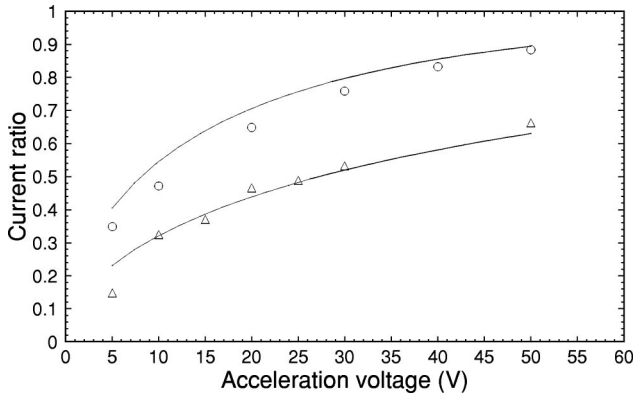

FIG. 8. Measured fractions of emission current transmitted through the interaction electrodes (circles) and arriving at the collector (triangles) as functions of the acceleration voltage U_0, compared to the modeled thermal broadening (lines) using the rms Gaussian widths of Sec. III B scaled up by 10%.

rent distribution of 4 mm height (as determined from the space-charge flow simulation) is convoluted with a Gaussian of the width calculated for the respective flight times from the cathode, which increase $\propto U_0^{-1/2}$ for decreasing acceleration voltage U_0 (cf. Sec. III B). These convoluted profiles are integrated up to the limits of the relevant apertures (± 6.5 mm for the transmitted current ratio and ± 3.75 mm for the collector current ratio). A reasonable representation of the measured current ratios is obtained if the calculated Gaussian widths of Sec. III B are scaled up by 10%. In view of the roughness of the model, we consider that the observed current ratios are consistent with the expected spatial broadening of the electron beam due to thermal effects.

Regarding the effect of stray magnetic fields, the strongest sensitivity is to transverse fields (i.e., perpendicular to the plane of Fig. 4). At 50 eV, fields of ~ 0.04 mT in this direction are found to reduce the collector current by about a factor of 2. Comparable effects of magnetic field components in the other directions occur at about one order of magnitude higher fields strengths.

The 50 eV electron beam produced in the electron gun could be imaged optically[22] at the nominal current using a Willemit phosphor screen[29] in place of the collector. Such observations were hampered by short lifetimes of the phosphor layer (<30 min). The light intensity distribution, observed on a Peltier-cooled CCD camera, revealed a diffuse boundary of the electron beam, roughly consistent with the estimated thermal spreading at 50 eV (FWHM beam height 7.5 ± 1 mm, beam width 60 ± 2 mm).

IV. MEASUREMENT PROCEDURE

A. Trapping cycle

The measurement cycle starts by opening the chopper at the ion source for several tens of microseconds (the dc beam from the source is chopped in order to reduce the background of neutrals produced before the trap[15]). These ions, usually at an energy of 4.2 keV, are mass selected by both a 20° magnet near the source and a 90° magnet about halfway between the source and the ion trap. Once the ion trap is filled (as can be verified with the pickup), the voltages of the entrance mirror electrodes are raised and the beam is trapped.

Neutral particles produced either by collisions with the residual gas (background) or by the electron beam (signal) and moving downstream are counted using the MCP (see Fig. 1). In order to separate the signal from the background, the electron beam was modulated at a rate of 20 Hz, 20% of the cycle with electrons "on" and 80% with electrons "off." The clock gating the electron beam was not synchronized with the trapping cycle so that all trapping times were probed equally. A measuring cycle usually comprises 10 injections at the same electron energy, plus one injection for normalization purposes (see Sec. IV C). For each injection, the beam is trapped for a time that is comparable with the beam lifetime. The entrance mirror is then grounded for 200 ms, during which the rate without ion beam is measured. All parameters are computer controlled, and the energy of the electron beam is scanned from 5 eV, by steps of 1 eV, up to 30 eV. At this point the scan is reversed and the energy steps are set to -1 eV. The scanning runs continuously until enough statistics have been accumulated. The data are recorded by a computer after each injection. This procedure allows checking for any systematic errors due to a possible change in the background pressure induced by different electron currents.

B. Cross section measurement

One of the main problems in measuring a collision cross section with the electrostatic ion trap setup is the normalization procedure. In order to obtain a relative cross section for different ionic species, both the electron and ion currents must be known. As pointed out in Sec. III D, it is assumed that the current measured by the collector of the electron target is proportional to the current passing through the interaction region, and this number can be used directly for normalization. The most difficult issue is the normalization to the number of trapped ions. In a single pass experiment, this value is determined by measuring the incoming current, after the interaction region, using a Faraday cup. Since this procedure is not feasible in the ion beam trap, we describe in Sec. IV C a new procedure which allows us to extract relative cross sections with high precision.

First, we describe the more common determination of the cross section from a crossed beam measurement. To that end, let us define the number of neutrals per unit time measured by the MCP when the electron beam is on as R_{on} and when the electron beam is off as R_{off}. Thus, the ratio between the rate of production of neutrals by the electron beam, R_e, and the background rate, R_b, of the neutrals produced by collision with the residual gas is given by

$$F = \frac{R_e}{R_b} \equiv \frac{R_{\mathrm{on}} - R_{\mathrm{off}}}{R_{\mathrm{off}}}. \tag{2}$$

In a crossed-beam geometry, the rate of neutralization due to collisions with electrons, measured by a detector with a detection efficiency η, is given by[30]

$$R_e = \frac{\eta \sigma_e I_e I_i}{|q| e^2 f_e} \frac{\sqrt{v_e^2 + v_i^2}}{v_e v_i}, \tag{3}$$

where σ_e is the cross section for electron induced neutralization, v_e and v_i are the electron and ion velocities, I_e and I_i are the electron and ion electrical currents, respectively, and $|q|$ is the ion charge number. The form factor f_e of two crossed beams [the electron beam with current density $j_e(y,z)$ propagating along x, and the ion beam with current density $j_i(x,z)$ propagating along y] is given by[30]

$$f_e = I_e I_i \Big/ \int \left(\int j_e(y,z)\,dy \right) \left(\int j_i(x,z)\,dx \right) dz. \tag{4}$$

Since in our case $v_e \gg v_i$, Eq. (3) can in good approximation be replaced by

$$R_e = \frac{\eta \sigma_e I_e I_i}{|q| e^2 f_e v_i}. \tag{5}$$

Using the target density n_b (molecules per unit area) of the residual gas, the background rate (electron beam "off") is given by

$$R_{\text{off}} \equiv R_b = \frac{\eta \sigma_b n_b I_i}{|q|e}, \tag{6}$$

where σ_b is the effective cross section for neutralization of the stored ions in collisions with the residual gas molecules. Thus, the cross section σ_e can be obtained from the ratio F measured according to Eq. (2) through the relation

$$\sigma_e = F\, \sigma_b n_b e v_i (f_e/I_e) \tag{7}$$

if σ_b, n_b, I_e, and f_e are known. The quantity f_e/I_e can be obtained to good approximation from the measured collector current, as argued in Sec. IV D. The background target constant $\sigma_b n_b$, giving the proportionality between the electrical ion current and the background rate, has to be established in close temporal proximity to the electron cross section measurement, using direct electrical measurements of the stored ion current. In fact, the neutralization cross section σ_b sensitively depends on the ion under study[10] and on the residual gas composition, and cannot be universally predicted. Moreover, the residual gas target density is difficult to determine from direct current measurement and may change by electron stimulated desorption. Hence, while the background rate R_{off} provides the primary normalization via Eq. (7), an additional procedure is applied intermittently at short time intervals to normalize R_{off} versus the electrical ion current I_i.

C. Ion current normalization

For the ion current normalization, the number of trapped ions (or a value proportional to that number) needs to be measured. Techniques for measuring the number of stored particles have been developed for heavy-ion storage rings,[6] but these are not directly applicable in the present case, as the trap is operated in a mode in which the net current in the trap is zero (the ions move randomly back and forth). In order to overcome this problem, we bunch the ions so that the number of ions stored in the trap (independent of the ionic species) can be determined using the pickup electrode shown in Figs. 1 and 2. The signal measured on this electrode is then compared to the background rate R_b measured on the MCP detector, which thereby is normalized to the electrical ion current. As described in Sec. II the bunches are generated by applying a small rf voltage to one of the exit electrodes at the natural oscillation frequency of the ions in the trap, $f_0 \equiv \omega_0/2\pi \equiv 1/T_0$. The strength of the driving rf signal was set to 10 V peak-to-peak, which was found to be enough to have all the trapped ions in the bunch. The trap is made to work in such a mode once every ten injections, so that normalization is performed many times during the whole experimental cycle, minimizing the effects of pressure changes in the trap and any other drifts. The voltage signal from the pickup is a train of Gaussian-type pulses, each of which can be represented by

$$S_j(t) = \frac{A(t)}{\sqrt{2\pi}\Gamma} \exp\left(-\frac{[t-t_j]^2}{2\Gamma^2}\right), \tag{8}$$

where t_j is the time at which the center of the bunch passes through the pickup electrode, Γ is the temporal bunch width, and $A(t)$ is the area under the peak that is proportional to the number of ions in the bunch, $N_i(t)$, which varies during the trapping time[20]

$$A(t) = \frac{L_p}{C}\frac{e}{v_i} N_i(t). \tag{9}$$

Here, the pickup sensitivity, for singly charged ions, is expressed by the ratio of its length L_p (8 mm) to the total capacitance C ($\sim$5 pF, depending on the input capacitance of the preamplifier used[20]).

Instead of obtaining the peak area for each pickup pulse, which would require a lengthy fitting and background subtraction procedure to be run online, the amplified and digitized signal $S(t)$ is recorded for a time T_r=420 ms, and analyzed by calculating its Fourier transform. Individual bunch signals, described by Eqs. (8) and (9), are detected twice each trap period T_0. The resulting bunch signal in the time domain can be written as

$$S(t) = A(t) f(t) \tag{10}$$

with the periodic bunch sequence (extended from a large number of bunches to infinity for simplicity)

$$f(t) = \sum_{j=-\infty}^{\infty} \frac{1}{\sqrt{2\pi}\Gamma} \exp\left(-\frac{[t-jT_0]^2}{2\Gamma^2}\right) + \sum_{j=-\infty}^{\infty} \frac{1}{\sqrt{2\pi}\Gamma} \exp\left(-\frac{[t-(j+\kappa)T_0]^2}{2\Gamma^2}\right). \tag{11}$$

The first term of $f(t)$ describes a bunch passing through the pickup in the forward direction and the second term describes the bunch as it passes through the pickup in the opposite direction after a delay κT_0, where κ is a number between 0 and 1. The Fourier transform $\tilde{S}(\omega)$ of $S(t)$ is the convolution of the Fourier transforms $\tilde{A}(\omega)/2\pi$ and

$$\tilde{f}(\omega) = \omega_0\left(1 + e^{-i\kappa T_0 \omega}\right)\exp\left(-\frac{(\omega\Gamma)^2}{2}\right)\sum_{n=-\infty}^{\infty} \delta(\omega - n\omega_0), \tag{12}$$

of $A(t)$ and $f(t)$, respectively. In particular, the peak amplitude of the nth harmonic $\tilde{S}_n(\omega)$ [representing the nth term in the sum of Eq. (12)] is given by

$$|\tilde{S}_n(n\omega_0)| = \frac{\tilde{A}(\omega=0)}{T_0}\sqrt{2+2\cos(2\pi n\kappa)} \times \exp\left(-\frac{(n\omega_0\Gamma)^2}{2}\right) \tag{13}$$

with

$$\tilde{A}(\omega=0) \equiv \int_{-\infty}^{\infty} A(t)\exp(-i\omega t)dt = \frac{L_p}{C}\frac{e}{v_i}\int_0^{T_r} N_i(t)dt. \tag{14}$$

In general, the forward–backward sequence as characterized by the delay factor κ results in an irregular, interference–like pattern of the harmonic amplitudes [for a pickup in the center position of a symmetric trap (κ=0.5), odd harmonics would vanish and even harmonics would acquire an additional factor of 2 in their amplitude]. In our setup the pickup

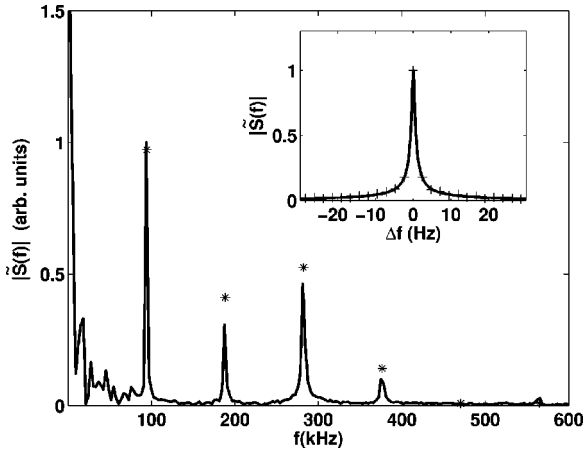

FIG. 9. FFT spectrum of the bunch signal of C_4^- (solid line), with the first harmonic normalized to unity. The spectrum is compared to the expected peak intensity of each harmonic given by Eq. (13) (*). The insert shows the peak shape of the first harmonic (+) and the fitted line shape (square root of a Lorentzian).

is situated close to the exit mirror with $\kappa=0.31$. Experimentally, and as expected from simple arguments, the relative bunch width is $\Gamma/T_0\approx 0.086$, so that the quantity $\omega_0\Gamma \approx 0.54$ is a constant that does not depend on the ion species for a given energy spread from the ion source and ion trap parameters. This leads to a decaying amplitude of the higher harmonics because of the exponential decay term, $\exp(-[(n\omega_0\Gamma)^2/2])$ in Eq. (13). The first harmonic amplitude, in contrast, is only weakly sensitive to Γ. Figure 9 shows the measured FFT spectrum compared to the expected harmonic behavior given Eq. (13). The shape of the FFT peak is described by $\tilde{A}(\omega)$. For the case of an exponentially decaying ion number $N_i(t)=N_0\exp(-t/\tau)$ with a lifetime τ, $\tilde{A}(\omega)$ can be well represented by the square root of a Lorentzian with a characteristic width $1/\tau$, given that $T_r >> T_0$, as demonstrated in the insert of Fig. 9 for the first harmonic fitted with $\tau=370\pm 20$ ms. This value compares well with the value of 300 ± 20 ms determined by fitting an exponential decay to the measured rate on the MCP detector. The lifetime with the rf on is about a factor of 2 shorter than without it, which was determined to be $\tau=600\pm 10$ ms from the MCP detector data, due to additional ion losses caused by the bunching process.

For the normalization of the cross section measurements we count the number of background neutral particles, N_b, at the MCP detector during the same time T_r as the pickup signal is acquired. Using the relation $I_i(t)=|q|eN_i(t)/T_0$ for the (average one-way) ion current and an exponentially decaying number of trapped ions, one obtains from Eq. (6)

$$N_b=\int_0^{T_r} R_b dt=\frac{\eta\sigma_b n_b}{T_0}\int_0^{T_r} N_i(t)dt. \tag{15}$$

On the other hand, Eqs. (13) and (14) yield

$$|\tilde{S}(\omega_0)|=\frac{\alpha}{v_i T_0}\int_0^{T_r} N_i(t)dt \tag{16}$$

with

$$\alpha=\frac{eL_p}{C}\sqrt{2+2\cos(2\pi\kappa)}\exp\left(-\frac{(\omega_0\Gamma)^2}{2}\right). \tag{17}$$

Hence, from the ratio of the background counts to the first-harmonic amplitude, the background target constant $\sigma_b n_b$ can be determined to be

$$\sigma_b n_b=\frac{\alpha}{\eta v_i}\frac{N_b}{|\tilde{S}(\omega_0)|} \tag{18}$$

and the electron collision cross section of Eq. (7) can be expressed as

$$\sigma_e=F\frac{\alpha}{\eta}\frac{N_b}{|\tilde{S}(\omega_0)|}\frac{ef_e}{I_e}. \tag{19}$$

From Eqs. (13), (14), and (15) it is obvious that the detailed time dependence of the trapped ion number, $N_i(t)$, cancels in the final result for the calibration factor α [Eq. (17)]. It is important to realize that, as long as the relative bunch width can be kept small, all the relevant quantities in α are geometrical or natural constants, characteristic of the ion trap system and independent of the ion mass and velocity. Moreover, for a given ion beam energy the trap optics, and hence the form factor f_e, are independent of the ion mass. Thus, through the described normalization procedure it is possible to compare directly electron impact cross sections for different ionic species with high relative precision.

When relative cross sections of several species are compared at the same electron energy, the main sources of error (except for statistics, which were found to be about 10%) are related to possible variations in (i) "pickup sensitivity," α, and (ii) detection efficiency of the MCP detector, η, for the different species. We estimate the first source of error to be less than 5%, due mainly to variations in bunch width. The detection efficiency of MCP detectors is known to depend on the impact energy and mass of the detected particle.[31] Applying Eq. (26) from this reference we estimate a reduction in detection efficiency of less than 10% for C_{15}^- and much less for smaller clusters. Therefore, the contribution of the variation of the detection efficiency with mass to the overall error is negligible. Finally, the overall accuracy of the relative cross section measurements is about 10%.

This experimental technique can be extended, in principle, to the measurement of absolute electron impact cross sections if fragmentation is negligible. To that end, a careful absolute calibration of the system is needed (this includes evaluating the pickup sensitivity and the detector efficiency, for example). Measurements for stored ions which fragment following the electron detachment, in contrast, require additional development of the experimental technique presented here. Although fragmentation of negative carbon and aluminum clusters following electron detachment is negligible, we did not pursue this direction because the measurement of absolute cross sections was not the primary focus of this work; instead we used existing C_2^- data[32] to determine the absolute cross sections.

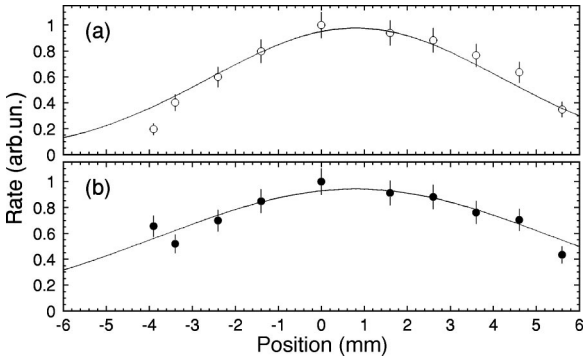

FIG. 10. Normalized electron-induced neutralization rates measured for C_2^- for different vertical positions of the electron target (zero relates to the axis of the trap mirrors) at (a) 40 eV and (b) 20 eV (circles). The lines give profiles calculated for an ion beam of 3 mm diam, uniform density and the thermally broadened electron beam profile (rms spreading 2.8 mm $\times(50\ \mathrm{eV}/E_e)^{1/2}$); the heights and an offset position (+0.8 mm for both curves) were chosen to fit the data. (The error bars represent typical counting errors.)

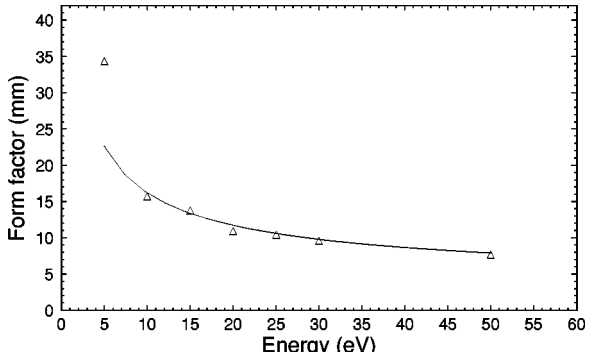

FIG. 11. Form factor f_e as a function of the electron energy as calculated (solid line) for thermally broadened electron beam profiles at the electron-ion interaction region (rms spreading 2.8 mm $\times(50\ \mathrm{eV}/E_e)^{1/2}$) and for a 3 mm diam ion beam of uniform density. The triangles show the form factor derived from the measured ratio of collector current to emission current (see text) with an energy-independent scale factor of $f_e'=5.1$ mm.

D. Form factor and electron current normalization

The electron current fractions transmitted through the interaction electrodes and through the collector entrance (Sec. III D) gave evidence for substantial spatial spread of the electron beam and could be reasonably simulated by considering the transverse thermal velocities at the cathode. This suggests that the electron beam in the interaction region should be considerably wider than obtained from the space-charge flow calculations. A corresponding result was obtained from measurements of electron-induced neutralization rates as a function of the vertical position of the electron target (Fig. 10), using C_2^- ions stored at 4.2 keV. For these measurements the background subtraction and a normalization to the electrical ion current were performed as described in the previous section. The ion beam size (although not accurately known) should not exceed ~3 mm diam, as concluded from ion trajectory calculations (cf. Sec. II); hence, the observed interaction profiles clearly indicate a broad electron beam profile.

The interaction profiles were modeled by convoluting the relevant beam current distributions [equivalent to the form factor calculation of Eq. (4)], assuming a variable vertical offset between the beams and the thermal spread as expected from the cathode temperature and the beam energy (see Sec. III D). For the two energies shown in Fig. 10 the data are well reproduced by the modeled profiles for the corresponding electron energies. They are hence consistent with the energy-dependent broadening of the interaction profile as predicted for thermal spread. The comparison of the model with the measured interaction profiles indicates that the vertical electron beam profile in the interaction region can be described by the convolution of a rectangular profile (4 mm high) with a Gaussian with a rms spread of 2.8(3) mm, corresponding to the estimated value of Sec. III D. Although these data give a direct measure of the electron beam width in the interaction region, they would not by themselves clearly indicate an energy-dependent broadening. The main evidence for such energy dependence stems from the current ratio measurements discussed in Sec. III D.

Using the modeled electron beam profile in the interaction region, the form factor f_e (for zero vertical offset between electron and ion beam) can be calculated as a function of energy as shown in Fig. 11. Since the electron beam height is large compared to the gap between the shielding electrodes (± 3.75 mm), the collector current I_c should sample the central current density in the interaction region as expressed by I_e/f_e, letting I_e denote the total current emitted by the cathode; hence, it should be possible to write $I_c = f_e'(I_e/f_e)$ with an energy-independent factor f_e'. As shown in Fig. 11, the modeled form factor f_e is indeed well reproduced by the inverse collector current ratio,

$$f_e = f_e'(I_e/I_c), \tag{20}$$

with $f_e'=5.1\pm0.2$ mm at all energies except the lowest point at 5 eV. The ratio of this beam gap between the shielding electrodes is 0.68 ± 0.03, close to the ratio between the distances from the cathode to the interaction region and to the collector entrance (0.63, see Sec. III D), which would be relevant for a diverging beam starting at the cathode center.

From these observations it appears adequate to monitor the effective electron current density in the interaction region by measuring the collector current I_c. The electron collision cross section is then given by modifying Eq. (19) to

$$\sigma_e = F\frac{\alpha}{\eta}\frac{N_b}{|\tilde{S}(\omega_0)|}\frac{ef_e'}{I_c} \tag{21}$$

with the energy-independent form factor f_e' given above. It should be noted that this form factor is largely independent of the ion beam diameter (as long as it stays below ~5 mm) and the ion beam profile (since the profile of the thermally spread electron beam is essentially flat over a few mm). Moreover, the trapping conditions between the electrostatic mirrors are independent of the ion mass for a given ion energy. Monitoring the effective electron density by the method applied here, one can expect to obtain high precision relative electron impact cross sections over a wide range of ion masses that, among others, is of interest for cluster studies.

Based on the agreement found between measured electron beam properties and their modeling, we estimate the uncertainty in the procedure implied by Eq. (21) to be about

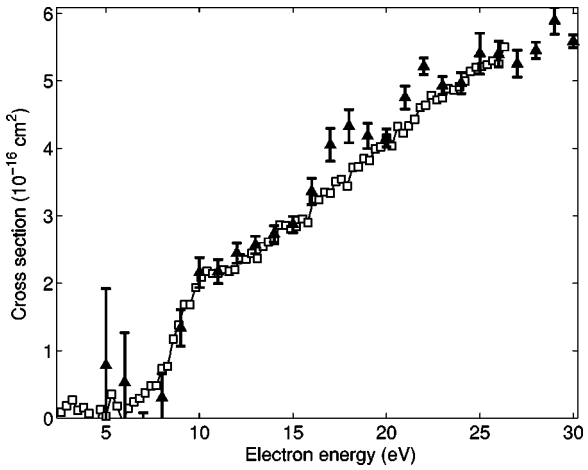

FIG. 12. Electron impact detachment cross section of C_2^- as a function of electron energy. The open squares are the results from the ASTRID storage ring (Ref. 32), and the triangles are the present results. The ion trap data are scaled to coincide at 20 eV.

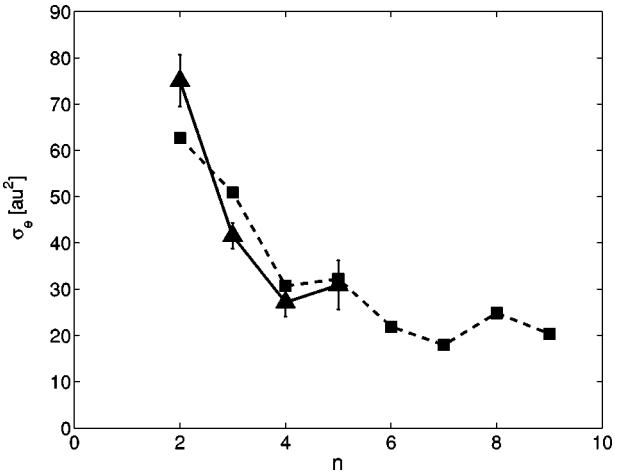

FIG. 13. Electron impact detachment cross section at 20 eV for Al_n^-(n =2–5) as a function of the cluster size, n, normalized to the cross section of C_2^- measured at 20 eV by Pedersen *et al.* (Ref. 32). Triangles: experimental results; squares: theoretical prediction (Refs. 35 and 36).

20% at energies above 10 eV. For lower energies the direct measurement of the collector current could still be suitable for obtaining the effective electron density, in spite of the discrepancy with the model calculation seen at 5 eV in Fig. 11, which possibly arises from an inadequate description of the beam spreading at this low energy. The uncertainties at energies <10 eV are difficult to assess without further investigation.

V. FIRST EXPERIMENTAL RESULTS

In order to test the complete setup, we have measured the relative electron impact detachment cross section of C_2^- in the energy range between 5–30 eV. This ion was chosen because it has been thoroughly studied using the ASTRID storage ring,[32–34] and its cross section shows a broad resonance at low energy ($E \sim 10$ eV). Thus, comparison between our measurement and those at ASTRID should allow us to test our normalization procedure, especially the assumed proportionality of the measured collector current to the effective electron density seen by the ion beam, as well as our ability to measure reactions at relatively low electron energy. Figure 12 shows the comparison between the ASTRID data (open squares)[32] and the electrostatic trap data (triangles), with the latter scaled to coincide with the former at 20 eV. It can be seen that there is excellent agreement between the two, and that the low energy resonance is reproduced nicely by the electrostatic trap measurement. It is important to point out that this comparison demonstrates that the electron energy, current and form factor are well under control in the ion trap.

Systematic studies of electron impact detachment from negative clusters are underway in our laboratory. The electron detachment cross sections of Al_n^- clusters, for $2 \leqslant n \leqslant 5$, bombarded by 20 eV electrons are shown in Fig. 13. The data (triangles) are in good agreement with the theoretical predictions (squares) based on the model of Andersen *et al.*[35,36] Both experimental and theoretical cross sections were normalized to the C_2^- cross section measured by Pedersen *et al.*[32] and shown in Fig. 12. Note the high precision obtained for the relative cross sections of the different cluster ions. Details about these results will be given in a forthcoming publication.[37]

ACKNOWLEDGMENTS

The authors would like to thank Y. Shachar for his help during the installation of the trap. The cooperation of Tom Deany at Nor-Cal in producing the optical table is appreciated. The work is supported by the Israel Science Foundation and by the German Israel Foundation for Scientific Research (GIF) under Contract No. I-707-55.7/2001. I.B.I. is partly supported by the Chemical Sciences, Geosciences and Biosciences Division, Office of Basic Energy Sciences, Office of Science, U.S. Department of Energy.

[1] K. T. Dolder and B. Peart, Rep. Prog. Phys. **39**, 693 (1976).
[2] B. Peart, R. Forrest, and K. T. Dolder, J. Phys. B **12**, 847 (1979).
[3] A. E. Bannister, H. F. Krause, C. R. Vane, N. Djuric, D. B. Popovic, M. Stepanovic, G. H. Dunn, Y. S. Chung, A. C. H. Smith, and B. Wallbank, Phys. Rev. A **68**, 042714 (2003).
[4] E. M. Bahati, J. J. Jureta, D. S. Belic, H. Cherkani-Hassani, M. O. Abdellahi, and P. Defrance, J. Phys. B **34**, 2963 (2001).
[5] D. Hathiramani, K. Aichele, W. Arnold, K. Huber, E. Salzborn, and P. Scheier, Phys. Rev. Lett. **85**, 3604 (2000).
[6] D. Habs *et al.*, Nucl. Instrum. Methods Phys. Res. B **43**, 390 (1989).
[7] S. P. Møller, in *Proceedings of the 1993 Particle Accelerator Conference*, Washington, D.C. 1993, edited by S. T. Corneliusseb , p. 1741.
[8] K. Abrahamsson *et al.*, Nucl. Instrum. Methods Phys. Res. B **79**, 269 (1993).
[9] M. Larsson, in *Gas Phase Ion Chemistry*, edited by N. G. Adams and L. Babcock (JAI, Greenwich, 2002), Vol. 4, p. 179.
[10] H. Shen, C. Brink, P. Hvelplund, and M. O. Larsson, Z. Phys. D: At., Mol. Clusters **40**, 371 (1997).
[11] A. Le Padellec, F. Rabilloud, D. Pegg, A. Neau, F. Hellberg, R. Thomas, H. T. Schmidt, M. Larsson, H. Danared, A. Källberg, K. Andersson, and D. Hanstorp, J. Chem. Phys. **115**, 10671 (2001).
[12] S. P. Møller, Nucl. Instrum. Methods Phys. Res. A **394**, 281 (1997).
[13] T. Tanabe, K. Chida, K. Noda, and I. Watanabe, Nucl. Instrum. Methods Phys. Res. A **482**, 595 (2002).
[14] D. Zajfman, O. Heber, L. Vejby-Christensen, I. Ben-Itzhak, M. Rappaport, R. Fishman, and M. Dahan, Phys. Rev. A **55**, R1577 (1997).
[15] M. Dahan, R. Fishman, O. Heber, M. Rappaport, N. Altstein, D. Zajfman, and W. J. van der Zande, Rev. Sci. Instrum. **69**, 76 (1998).
[16] S. Boye, H. Krogh, I. B. Nielsen, S. B. Nielsen, S. U. Pedersen, U. V. Pedersen, L. H. Andersen, A. F. Bell, X. He, and P. J. Tonge, Phys. Rev.

Lett. **90**, 118103 (2003).
[17] T. Tanabe, K. Noda, M. Saito, S. Lee, Y. Ito, and H. Takagi, Phys. Rev. Lett. **90**, 193201 (2003).
[18] H. Bluhme, M. J. Jensen, S. B. Nielsen, U. V. Pedersen, K. Seiersen, and L. H. Andersen, Phys. Rev. A **70**, 020701 (2004).
[19] H. B. Pedersen, D. Strasser, O. Heber, M. L. Rappaport, and D. Zajfman, Phys. Rev. A **65**, 042703 (2002).
[20] H. B. Pedersen, D. Strasser, B. Amarant, O. Heber, M. L. Rappaport, and D. Zajfman, Phys. Rev. A **65**, 042704 (2002).
[21] SAES Getters S. P.A., Lainate (Milano), Italy.
[22] P. D. Witte, Ph.D. thesis, University of Heidelberg, 2002, www.ub.uniheidelberg.de/archiv/2977 (unpublished).
[23] P. T. Kirstein, G. S. Kino, and W. E. Waters, *Space-Charge Flow* (McGraw–Hill, New York, 1967), p. 140.
[24] W. B. Herrmannsfeldt, Electron Trajectory Program, SLAC-226, Stanford, 1979.
[25] J. R. Pierce, *Theory and Design of Electron Beams* (Van Nostrand, New York, 1954).
[26] T. Weiland *et al.*, in *Computational Accelerator Physics*, edited by J. J. Bisognano and A. A. Mondelli, AIP Conf. Proc. Vol. 391 (AIP, New York, 1997), p. 65; CST (Gesellschaft fur Computer-Simulationstechnik GmbH), Darmstadt, Germany.
[27] J. L. Cronin, Proc. IEEE 128, Pt. I, No. 1, Feb. 1981.
[28] Cathode manufactured by Heatwave Labs, Inc., Watsonville, CA.
[29] W. Espe, *Werkstoffkunde der Hochvakuumtechnik* (Dt. Verl. der Wissenschaften, Berlin, 1962); Bd. III; sample coating courtesy Leuchtstoffwerk Heidelberg.
[30] M. F. A. Harrison, in *Methods of Experimental Physics*, edited by B. Bederson and W. L. Fite (Academic, New York, 1968), Vol. 7A, p. 95.
[31] G. W. Fraser, Int. J. Mass. Spectrom. **215**, 13 (2002).
[32] H. B. Pedersen, N. Djuric, M. J. Jensen, D. Kella, C. P. Safvan, H. T. Schmidt, L. Vejby-Christensen, and L. H. Andersen, Phys. Rev. A **60**, 2882 (1999).
[33] L. H. Andersen, P. Hvelplund, D. Kella, P. H. Mokler, H. B. Pedersen, H. T. Schmidt, and L. Vejby-Christensen, J. Phys. B **29**, L643 (1996).
[34] H. B. Pedersen, N. Djuric, M. J. Jensen, D. Kella, C. P. Safvan, L. Vejby-Christensen, and L. H. Andersen, Phys. Rev. Lett. **81**, 5302 (1998).
[35] L. Vejby-Christensen, D. Kella, D. Mathur, H. B. Pedersen, H. T. Schmidt, and L. H. Andersen, Phys. Rev. A **53**, 2371 (1996).
[36] L. H. Andersen, in *Photonic, Electronic, and Atomic Collisions - 22nd International Conference*, edited by J. Burgdörfer, J. S. Cohen, S. Datz, and C. R. Vane (Rinton, Princeton, 2002), p. 292.
[37] A. Diner, Y. Toker, D. Strasser, O. Heber, I. Ben-Itzhak, P. D. Witte, A. Wolf, D. Schwalm, M. L. Rappaport, K. G. Bhushan, and D. Zajfman, Phys. Rev. Lett. **93**, 063402 (2004).